arXiv:1011.0049v2 [cond-mat.str-el] 31 Mar 2011

Metal-Insulator Transition and Magnetic Order in the Pyrochlore Oxide $Hg_2Ru_2O_7$

Makoto YOSHIDA*, Masashi TAKIGAWA†, Ayako YAMAMOTO[1], and Hidenori TAKAGI[1,2]

Institute for Solid State Physics, University of Tokyo, Kashiwa, Chiba 277-8581
[1]*RIKEN Advanced Science Institute, Wako, Saitama 351-0198*
[2]*Department of Advanced Materials, University of Tokyo, Kashiwa, Chiba 277-8561*

We report results of NMR experiments on the ruthenium oxide $Hg_2Ru_2O_7$ with the pyrochlore structure, which exhibits a metal-insulator transition at $T_{\rm MI} = 107$ K. In the metallic phase above $T_{\rm MI}$, the nuclear spin-lattice relaxation rate $1/T_1$ and the Knight shift at the Hg sites follow the Korringa relation, indicating the absence of substantial spatial spin correlation. At low temperatures in the insulating phase, ^{99,101}Ru-NMR signals are observed at zero magnetic field, providing evidence for a commensurate antiferromagnetic order. The estimated ordered moment is about 1 μ_B per Ru, much smaller than 3 μ_B expected for the ionic $(4d)^3$ configuration of Ru^{5+}. Thus, the localized spin models are not appropriate for the insulating phase of $Hg_2Ru_2O_7$. We also discuss possible antiferromagnetic spin structures.

KEYWORDS: pyrochlore structure, ruthenium oxide, $Hg_2Ru_2O_7$, NMR, metal-insulator transition, magnetic order

1. Introduction

The pyrochlore lattice, a network of corner-sharing tetrahedra, is known for strong geometrical frustration.[1] Antiferromagnetically coupled localized spins on this lattice exhibit a massive degeneracy of low-energy states. Both classical[2–4] and quantum[5–7] spin systems on the pyrochlore lattice with the nearest neighbor Heisenberg interaction are believed to remain disordered down to zero temperature with spin liquid ground states. Real materials, however, have secondary interactions, which may stabilize a magnetic order. The effects of secondary interactions such as anisotropy,[8] longer range Heisenberg[2] or dipolar[9] interactions, Dzyaloshinsky-Moriya (DM) interaction,[10] and spin-lattice coupling[11,12]have been studied theoretically.

Although the concept of frustration is well established for localized spins, it is not yet clear for itinerant electron systems. Nevertheless, some anomalous properties of itinerant electrons on a pyrochlore lattice are considered to be related to geometrical frustration. A well-known example is the spinel oxide LiV_2O_4, where mixed valent V atoms form a pyrochlore lattice. This compound shows heavy-electron behavior such as extremely enhanced specific heat and magnetic susceptibility at low temperatures.[13] The origin could be the large degeneracy of low-lying states inherent to frustrated systems, and the mechanism of the heavy-electron behavior is probably different from the Kondo resonance in f-electron systems.[14]

Some pyrochlore oxides show metal-insulator (MI) transitions by changing temperature or pressure. Such materials may help us fill the gap of our understanding of the frustration effects of localized spins and itinerant electrons. The MI transition in $Cd_2Os_2O_7$ at $T_{\rm MI} = 226$ K is continuous with no change in structural symmetry.[15,16] The Slater mechanism was proposed to explain the transition, i.e., unit cell doubling due to an antiferromagnetic order below $T_{\rm MI}$ opens a gap at the Fermi level. In another example, $Tl_2Ru_2O_7$, the discontinuous MI transition is accompanied by a pronounced structural change at 120 K.[17–19] The low-temperature insulating phase has a spin-singlet ground state with a gap in magnetic excitations.[18] Lee *et al.* proposed that orbital ordering among $4d$ electrons of Ru^{4+} $(4d^4)$ ions stabilized by structural distortion results in the formation of effectively one-dimensional spin chains and interpreted the excitation gap as the Haldane gap of spin 1 Heisenberg chains.[19]

Recently, a MI transition has been reported in another Ru-pyrochlore oxide, $Hg_2Ru_2O_7$.[20–22] This compound shows a first-order MI transition with a hysteresis at $T_{\rm MI} = 107$ K. Upon cooling through $T_{\rm MI}$, the resistivity increases abruptly and the crystal structure changes from cubic to one of lower symmetry, although the structural refinement has not been performed yet in the low-temperature phase.[20] In the metallic phase above $T_{\rm MI}$, the magnetic susceptibility χ increases slightly with decreasing temperature but decreases discontinuously below $T_{\rm MI}$, suggesting either an antiferromagnetic order[21] or a spin-singlet ground state.[20] Although such behavior is similar to $Tl_2Ru_2O_7$, the valence of Ru in $Hg_2Ru_2O_7$ is 5+ with the $4d^3$ configuration and, in the localized picture, we expect a half filled t_{2g} manifold with spin 3/2 and no orbital degree of freedom. Therefore, the magnetic ground state should be quite different from $Tl_2Ru_2O_7$.

In this paper, we report results of NMR measurements in $Hg_2Ru_2O_7$ and discuss the microscopic magnetic properties. We found from ^{199}Hg-NMR that the metallic phase above $T_{\rm MI}$ does not exhibit substantial spatial magnetic correlation. ^{99,101}Ru-NMR lines are observed at zero field at low temperatures, providing evidence for an antiferromagnetic order in the insulating phase. The ordered moments are estimated to be about 1 μ_B per Ru. The small moment compared with the expected value (3 μ_B) from Ru^{5+} ($S = 3/2$) implies that the localized spin model with strong Hund's cou-

*E-mail address: yopida@issp.u-tokyo.ac.jp
†E-mail address: masashi@issp.u-tokyo.ac.jp

pling is inadequate to explain the magnetic properties of $Hg_2Ru_2O_7$.

2. Experiment

Powder samples of $Hg_2Ru_2O_7$ were prepared as described in ref. 20. Most of the NMR measurements were performed on sample A with natural isotopic abundance. We also prepared isotopically enriched sample B containing 97.7% ^{99}Ru for the unambiguous site assignment of NMR lines at zero magnetic field. For sample B, we first prepared RuO_2 by heating isotopically enriched Ru metal at 900 °C in air, followed by the same procedure used for sample A. Most of the NMR spectra of ^{199}Hg nuclei were obtained by summing up the Fourier transform of the spin-echo signal at equally spaced frequencies with a fixed magnetic field.[23] The NMR spectra of ^{99,101}Ru nuclei at zero magnetic field were obtained by recording the integrated intensity of the spin-echo signal at discrete frequencies. The nuclear spin-lattice relaxation rate $1/T_1$ was measured by the inversion recovery method. Various properties of nuclei relevant to the present study are summarized in Table I.

3. Results and Discussion

In §3.1, we present the results of ^{199}Hg-NMR, which indicate that $Hg_2Ru_2O_7$ above T_{MI} is a correlated metal with negligible spatial spin correlation. We also discuss the change in spectral shape and the loss of signal intensity across T_{MI}, pointing to a magnetic order in the insulating phase. In §3.2, we show the results of zero-field ^{99,101}Ru-NMR at low temperatures, providing direct evidence for an antiferromagnetic order below T_{MI}. Possible magnetic structures are discussed in §3.3.

3.1 ^{199}Hg-NMR

The NMR frequency ν_r of ^{199}Hg nuclei, which have spin 1/2 and no quadrupole moment, is expressed in the paramagnetic state as,

$$\nu_r = {}^{199}\gamma B(1+K), \tag{1}$$

where $^{199}\gamma$ is the gyromagnetic ratio of ^{199}Hg nuclei and B is the external magnetic field. The Knight shift K represents the shift in resonance frequency due to a magnetic hyperfine field induced by the external field. Since the Hg sites in the pyrochlore structure have trigonal symmetry $\bar{3}m$, the Knight shift should follow a uniaxial angular dependence,

$$K(\theta) = K_{\rm iso} + K_{\rm ax}\left(3\cos^2\theta - 1\right), \tag{2}$$

where θ is the angle between the local symmetry axis along the $\langle 111\rangle$ direction and the external field. For a powder sample, the NMR line shape represents the histogram $P(K)$ of the angular distribution of $K(\theta)$,

$$P(K) \propto \left|\frac{dK}{d\cos\theta}\right|^{-1} \propto |K - K_\perp|^{-1/2}, \tag{3}$$

for $K_\parallel \le K \le K_\perp$ or $K_\perp \le K \le K_\parallel$ and $P(K) = 0$ otherwise. Here, $K_\parallel = K_{\rm iso} + 2K_{\rm ax}$ and $K_\perp = K_{\rm iso} - K_{\rm ax}$ are the Knight shifts for a field parallel and perpendicular to the symmetry axis, respectively.

Table I. Nuclear spin I, gyromagnetic ratio γ_n, quadrupole moment Q, and natural abundance for ^{199}Hg and ^{99,101}Ru.

	I (MHz)	γ_n (MHz/T)	Q (barn)	abundance (%)
^{199}Hg	1/2	7.6258	–	16.9
^{99}Ru	5/2	1.9607	0.079	12.8
^{101}Ru	5/2	2.1975	0.457	17.1

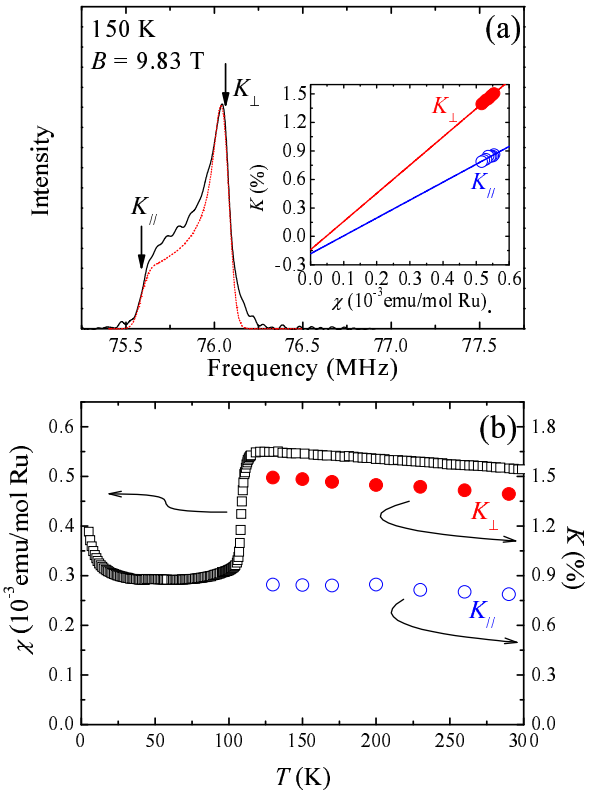


Fig. 1. (Color online) (a) ^{199}Hg-NMR spectrum in the metallic phase (T = 150 K) obtained for sample A in the magnetic field of 9.83 T ($^{199}\gamma B$ = 74.953 MHz). The red dotted line shows the fit to the powder pattern for an axially symmetric Knight shift. The edge and peak of the spectrum marked by $K_\parallel$ and $K_\perp$ respectively correspond to the resonance frequencies for the field parallel and perpendicular to the trigonal $\langle 111\rangle$ axis. In the inset, $K_\parallel$ and $K_\perp$ are plotted against the magnetic susceptibility χ (the $K-\chi$ plot) and fit to straight lines. (b) Temperature dependences of χ (open squares), $K_\parallel$ (open circles), and $K_\perp$ (solid circles).

Figure 1(a) shows a typical ^{199}Hg-NMR spectrum in the metallic phase above T_{MI}. The spectra can be fit reasonably well to eq. (3) convoluted with a gaussian broadening function as shown by the red dotted line. Figure 1(b) shows the temperature dependences of $K_\parallel$ and $K_\perp$, corresponding to the edge and peak positions of the spectrum, respectively, and the magnetic susceptibility χ of the same sample. Both the Knight shifts and susceptibility increase slightly with decreasing temperature.

The magnetic susceptibility χ is generally expressed as

$$\chi = \chi_0 + \chi_{\rm spin}(T), \tag{4}$$

where the first term is the sum of the diamagnetic and orbital (van-Vleck) contributions, which are independent of temperature, and the second term is the spin contri-

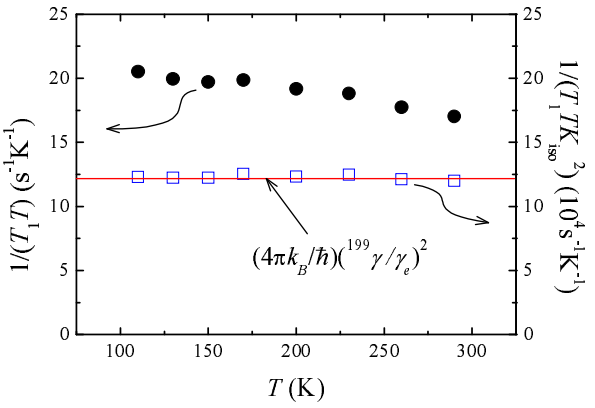


Fig. 2. (Color online) Temperature dependences of $1/(T_1T)$ (solid circles) and $1/(T_1TK_i^2)$ (open squares) at the Hg sites. The relaxation rate $1/T_1$ was measured at the peak frequency of the spectra in the field of 9.83 T. The solid line represents $S \equiv (4\pi k_B/\hbar)(^{199}\gamma/\gamma_e)^2$.

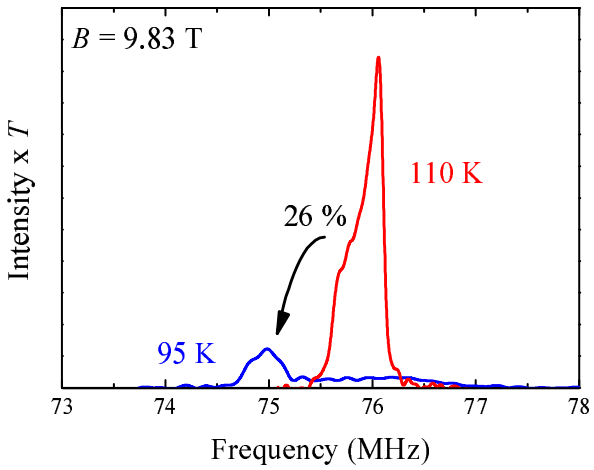


Fig. 3. (Color online) ^{199}Hg-NMR spectra at 95 and 110 K at 9.83 T. The vertical axis represents the spectral intensity multiplied by temperature.

bution, which may depend on temperature. Similarly,

$$K_\epsilon = K_{\epsilon,0} + K_{\epsilon,\mathrm{spin}}(T)\ (\epsilon = \ \parallel \text{ or } \perp), \tag{5}$$

where the first (second) term is the chemical (spin) shift. The spin part of the susceptibility (per mole of Ru) and the spin Knight shift are linearly related as

$$K_{\epsilon,\mathrm{spin}} = A_\epsilon^{\mathrm{Hg}} \frac{\chi_{\mathrm{spin}}}{N_A\mu_B}, \tag{6}$$

where A_ϵ^{Hg} is the hyperfine coupling between the conduction electron spin and the ^{199}Hg nuclei representing the magnetic hyperfine field produced by a uniform magnetization of 1 μ_B per Ru atom.

In the inset of Fig. 1(a), $K_\parallel$ and $K_\perp$ are plotted against χ (the K-χ plot) and fit to straight lines. The slopes of the lines give the hyperfine coupling constants $A_\parallel^{\mathrm{Hg}} = 10.5$, $A_\perp^{\mathrm{Hg}} = 16.6$ (T/μ_B) or equivalently $A_{\mathrm{iso}}^{\mathrm{Hg}} = 14.6$, $A_{\mathrm{ax}}^{\mathrm{Hg}} = -2.03$ (T/μ_B). Thus, the hyperfine interaction is mainly isotropic, indicating that the major source of the hyperfine field at the ^{199}Hg nuclei is the spin polarization on the Hg-s orbital hybridized with the conduction band. The chemical shift of ^{199}Hg nuclei is negative for most diamagnetic compounds and its absolute value is less than 0.3%,[24] when dimethil-mercury ($HgMe_2$) is used as the reference material. The value of $^{199}\gamma$ in Table I is also determined against $HgMe_2$ as the reference. Since this value is much smaller than the observed values of K_{iso}, we set $K_{\epsilon,0} = 0$ in eq. (5). The $K-\chi$ plot in the inset of Fig. 1(a) then indicates that $\chi \sim \chi_{\mathrm{spin}}$.

We next discuss the nuclear relaxation rate. For non-interacting electrons, K_{spin} and $1/(T_1T)$ (the nuclear spin-lattice relaxation rate $1/T_1$ divided by T) are basically temperature-independent and satisfy the following Korringa relation when the hyperfine field is due to s-electrons:

$$\frac{1}{T_1TK_{\mathrm{spin}}^2} = \frac{4\pi k_B}{\hbar}\left(\frac{\gamma_n}{\gamma_e}\right)^2 \equiv S, \tag{7}$$

where γ_e is the gyromagnetic ratio of electrons. Figure 2 shows the temperature dependence of $1/(T_1T)$ in $Hg_2Ru_2O_7$ at the ^{199}Hg sites measured at the peak frequency of the spectra. Unlike in simple metals, $1/(T_1T)$ increases slightly with decreasing temperature. Such an increase in $1/(T_1T)$ has often been ascribed to the electron-electron interaction causing the growth of low-energy spin fluctuations.[25] For instance, $1/(T_1T)$ at the Cu sites in high-T_c cuprate superconductors shows Curie-Weiss temperature dependence due to the development of antiferromagnetic spin fluctuations.[26] When the low-frequency spin fluctuations are associated with spatial correlation at a particular wave vector $\mathbf{q}$, $1/(T_1T)$ and K_{spin} are affected in different ways. If ferromagnetic correlation develops near $q = 0$, K_{spin} is enhanced much more strongly than $1/(T_1T)$, resulting in $1/(T_1TK_{\mathrm{spin}}^2)$ becoming significantly smaller than S in eq. (7). On the other hand, antiferromagnetic spin fluctuations at a non-zero q enhance $1/(T_1T)$, but do not substantially change K_{spin}, making $1/(T_1TK_{\mathrm{spin}}^2)$ much larger than S.

In Fig. 2, $1/(T_1TK_{\mathrm{iso}}^2)$ is plotted against temperature and compared with S for ^{199}Hg nuclei (the red line). Here, we consider only the isotropic component of K_{spin} due to s electrons and neglect the much smaller axial part. The result that $1/(T_1TK_{\mathrm{iso}}^2)$ is strictly independent of temperature with a value very close to S rules out strong spatial spin correlation at any specific wave vector. On the other hand, the density of states at the Fermi level calculated by the local-density approximation, $\rho = 3.7$ states/eV-Ru,[27,28] gives the bare spin susceptibility $\rho\mu_B^2 = 1.2\times10^{-4}$ emu/mol-Ru. Since the measured $\chi \sim 5.5\times10^{-4}$ emu/mol-Ru is dominantly due to a spin contribution, we conclude that χ_{spin} is enhanced by a factor of five. This modest enhancement of χ_{spin} and the absence of spatial spin correlation leads us to conclude that the spin fluctuations are local, i.e., largely uniform in $\mathbf{q}$-space. Such behavior is similar, for example, to that of the local Fermi liquid in Kondo systems.[29] We may also say that the temperature dependences of χ_{spin} and $1(/T_1T)$ should be ascribed to the variation in the effective density of states. The absence of spatial correlation in $Hg_2Ru_2O_7$ may be a manifestation of geo-

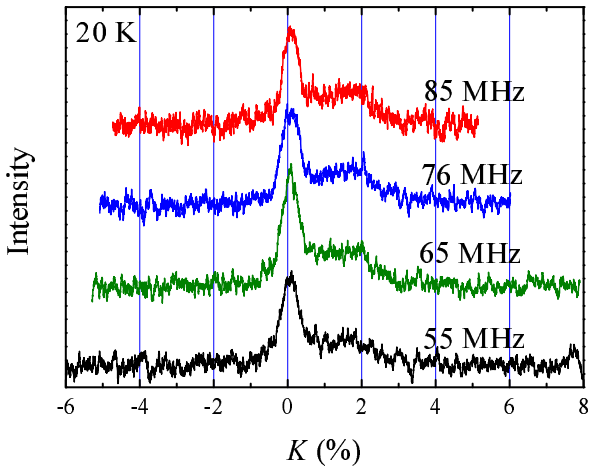


Fig. 4. (Color online) Field-swept ^{199}Hg-NMR spectra at 20 K obtained at different frequencies.

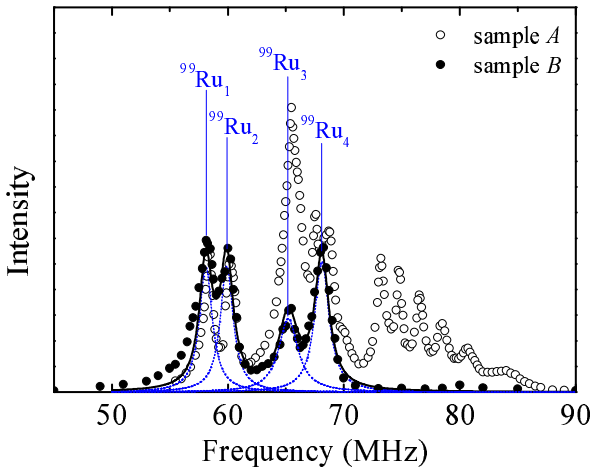


Fig. 5. (Color online) NMR spectrum at zero field obtained for sample A with natural isotopic abundance at T=1.6 K (open circles) and sample B enriched with ^{99}Ru isotope at T=4.2 K (solid circles). The solid line represents fitting to the spectrum from sample B by the sum of four Lorentzian functions with full widths at half maximum of 1.4, 1.4, 2.0, and 1.5 MHz for the ^{99}Ru$_1$, ^{99}Ru$_2$, ^{99}Ru$_3$, and ^{99}Ru$_4$ sites, respectively (dotted lines).

metrical frustration of the pyrochlore lattice in itinerant electron systems.

Let us now discuss the ^{199}Hg-NMR results in the insulating phase. Figure 3 shows the ^{199}Hg-NMR spectra above and below $T_{\rm MI}$. Significant changes in the spectral shape and intensity are observed.[30] The integrated intensity of the spectrum is reduced to 26% upon cooling across $T_{\rm MI}$, i.e., only one-quarter of the Hg sites contribute to the NMR signal in the frequency range between 74 and 78 MHz in the insulating phase. The resonance frequency of the rest of the Hg sites must be distributed over a much wider frequency range owing to the large hyperfine fields, suggesting a magnetically ordered state with spontaneous magnetic moments.

Figure 4 shows the ^{199}Hg-NMR spectra at 20 K at different frequencies. Here, the spectra were obtained by sweeping the magnetic field B at a fixed frequency and plotted against the fractional shift in the resonance field, $K = (\nu_r - {}^{199}\gamma B)/{}^{199}\gamma B$. Plotted in this way, all the spectra in Fig. 4 have identical line shapes, indicating that the hyperfine field $\nu_r - {}^{199}\gamma B$ is proportional to B. Therefore, for one-quarter of the Hg sites being observed, the hyperfine field from the spontaneous magnetic moments must be canceled out and the NMR line shape is determined solely by a small shift due to field-induced magnetization. The spectra in Fig. 4 have two components, a sharp peak at $K \sim 0$ and a broad structure with an edge at $K \sim 2$ %, with nearly equal integrated intensities, suggesting that two types of Hg sites with equal populations contribute to the spectra in Fig. 4.

If the loss of the NMR signal from three-quarters of the Hg sites is due to the spontaneous hyperfine field from ordered magnetic moments, we should be able to observe NMR signals from these Hg sites at zero magnetic field. We have searched zero-field NMR signals in the frequency range between 30 and 200 MHz at low temperatures below 4 K. However, no signal was observed except for the resonance from ^{99,101}Ru, which will be described in detail in §3.2. Since the ordered moment is estimated to be 1 μ_B/Ru, as will be explained in §3.2, we expect the zero-field Hg resonance to be in the range of 80 - 130 MHz if the moments were ferromagnetically aligned, on the basis of the hyperfine coupling constants determined above. However, a much smaller resonance frequency is expected for antiferromagnetic spin configurations due to the cancellation of a hyperfine field from different neighbors. Therefore, the actual resonance frequency in $Hg_2Ru_2O_7$ is likely to be lower than 30 MHz, which would be difficult to observe because of reduced NMR sensitivity at lower frequencies.

3.2 ^{99,101}Ru-NMR

In order to obtain direct evidence for a magnetic order below $T_{\rm MI}$, a search was conducted for the resonance at zero magnetic field caused by a spontaneous hyperfine field. We found NMR signals in the frequency range of 50 - 90 MHz. The NMR spectrum at zero field obtained for sample A with natural isotopic abundance is shown by the open circles in Fig. 5. This spectrum consisting of several sharp peaks provides unambiguous microscopic evidence for a commensurate antiferromagnetic order in the insulating phase below $T_{\rm MI}$. There are three species of NMR active nuclei, ^{199}Hg and ^{99,101}Ru, in $Hg_2Ru_2O_7$ (Table I). In order to assign the resonance lines to specific nuclear species, we have also performed zero-field NMR measurements on sample B enriched with the ^{99}Ru isotope. The spectrum from sample B is shown by the solid circles in Fig. 5. The isotopic enrichment results in a marked change of the spectrum. In particular, all the resonance lines above 70 MHz observed in sample A are absent in sample B. Therefore, they should be assigned to ^{101}Ru.

Since both ^{99}Ru and ^{101}Ru nuclei have spin I = 5/2, the electric quadrupole interaction between the nuclear quadrupole moments and the electric field gradient (EFG) should split the zero-field resonance into five equally spaced lines up to the first-order perturbation

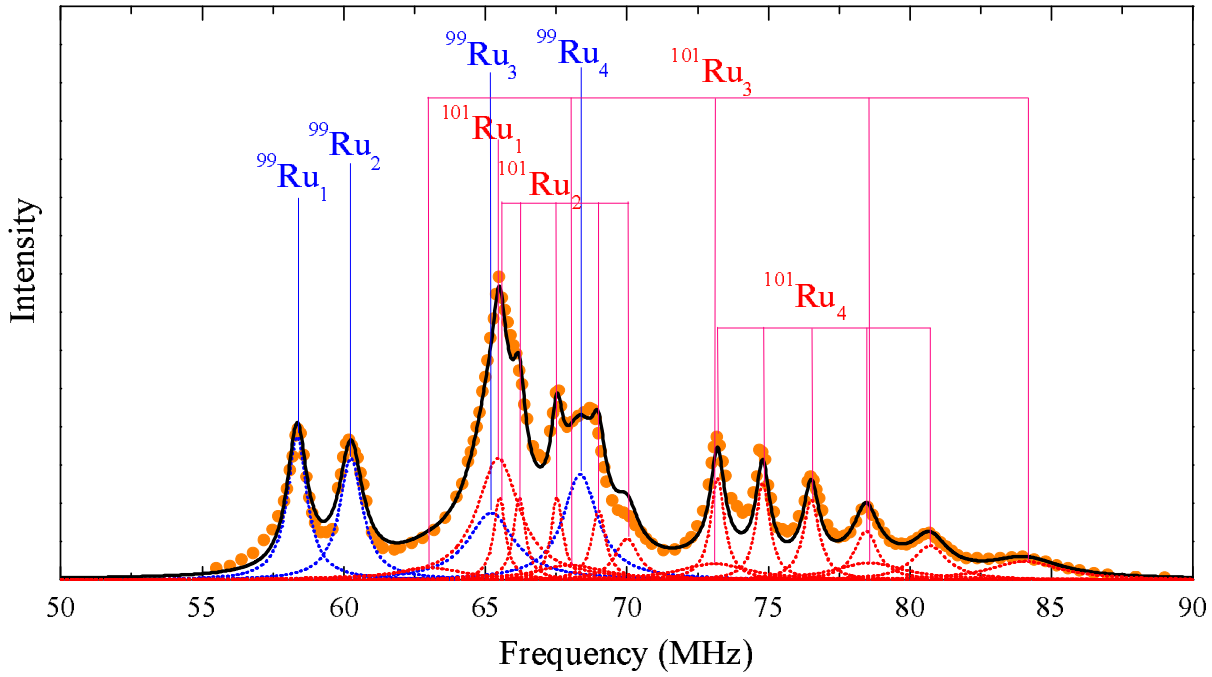


Fig. 6. (Color online) Zero-field NMR spectrum (solid circles) obtained for sample A at 1.6 K is reproduced by the sum of Lorentzian functions (solid lines), each of which (dotted lines) represents the peak from ^{99}Ru or ^{101}Ru nuclei on four inequivalent sites with equal populations.

in the quadrupole interaction. Since the Ru sites have the trigonal symmetry in $Hg_2Ru_2O_7$, the resonance frequency ν_M for the transition $I_z = M \leftrightarrow M-1$ is given as[31]

$$\nu_M = {}^{\alpha}\gamma B_{\rm hf}^{\rm Ru} + \frac{{}^{\alpha}\nu_q}{2}\left(3\cos^2\phi - 1\right)\left(M - \frac{1}{2}\right), \qquad (8)$$

where M takes five half-integer values between $-3/2$ and $5/2$, ${}^{\alpha}\gamma$ is the nuclear gyromagnetic ratio for ^{99}Ru ($\alpha = 99$) or ^{101}Ru ($\alpha = 101$), $B_{\rm hf}^{\rm Ru}$ is the magnitude of the hyperfine field from the spontaneous magnetic moments, and ϕ is the angle between $\mathbf{B}_{\rm hf}^{\rm Ru}$ and the trigonal axis of the Ru site being observed. The maximum quadrupole splitting ${}^{\alpha}\nu_q = 3e^{\alpha}QV_{zz}/[2I(I-1)h]$ is determined by the electric field gradient V_{zz} along the trigonal axis and the nuclear quadrupole moment ${}^{\alpha}Q$ of the ${}^{\alpha}$Ru nuclei.

We first examine the spectrum of sample B. The spectrum consists of four peaks, which should be assigned to ^{99}Ru. The non-uniform spacing between the peaks is in clear contradiction to the prediction of five equally spaced lines for a given $B_{\rm hf}^{\rm Ru}$. We therefore conclude that the quadrupole splitting for ^{99}Ru is too small to be resolved as distinct peaks. The peaks in the spectrum should then be assigned to four types of Ru sites with different values of $B_{\rm hf}^{\rm Ru}$. The spectrum from sample B is fit to the sum of four Lorentzian functions, as shown in Fig. 5. The four sites are labeled ^{99}Ru$_1$, ^{99}Ru$_2$, ^{99}Ru$_3$, and ^{99}Ru$_4$. The unresolved quadrupole splitting $|(\nu_q/2)(3\cos^2\phi - 1)|$ should contribute to the line width. ^{99}Ru$_3$ has the largest width, ^{99}Ru$_1$ and ^{99}Ru$_2$ have relatively small widths. On the other hand, the integrated intensities of these lines are almost the same, indicating equal populations of the four sites. The hyperfine field $B_{\rm hf}^{\rm Ru}$ for each site was obtained by dividing the peak frequency by ${}^{99}\gamma$ and is listed in Table II.

We now turn to the spectrum of sample A, which should contain resonance lines from four ^{101}Ru sites (^{101}Ru$_1$, ^{101}Ru$_2$, ^{101}Ru$_3$, and ^{101}Ru$_4$) in addition to the contribution of the four ^{99}Ru sites. Since ^{101}Ru nuclei have much larger quadrupole moments than ^{99}Ru, $^{101}Q/{}^{99}Q = 5.8$, quadrupole splitting may be well resolved in the spectrum of ^{101}Ru. Since the frequency of the center line ($M = 1/2$ in eq. 8) is not affected by the quadrupole interaction up to the first order, their positions for the ^{101}Ru sites are given by ${}^{101}\gamma B_{\rm hf}^{\rm Ru}$, where the values of $B_{\rm hf}^{\rm Ru}$ are listed in Table II. We have succeeded in reproducing the whole spectrum of sample A by adjusting the quadrupole splitting for the four ^{101}Ru sites, as indicated by the solid line in Fig. 6.

The values of the quadrupole splitting for the ^{101}Ru sites were determined as follows. First, one can easily recognize five lines with approximately uniform spacing in the frequency range of 73 - 81 MHz. Since the peak frequency of the center line agrees precisely with $B_{\rm hf}^{\rm Ru}$ at the ^{99}Ru$_4$ site multiplied by ${}^{101}\gamma$, these five lines are assigned to the ^{101}Ru$_4$ sites. We note, however, that the quadrupole splittings between adjacent lines are not completely uniform but take slightly different values, namely, 1.6, 1.7, 2.0, and 2.2 MHz from low to high frequencies. This should be due to the higher-order effects of the quadrupole interaction. Next, the difference of the spectra of the two samples between 63 and 72 MHz is attributed to the ^{101}Ru$_1$ and ^{101}Ru$_2$ sites, on the basis of the values of $B_{\rm hf}^{\rm Ru}$ of these sites. The spectral shape in this frequency range is well reproduced by assigning a very small unresolved quadrupole splitting less than 0.5 MHz to the ^{101}Ru$_1$ sites and a barely resolved small splitting of 1 MHz to the ^{101}Ru$_2$ sites, as indicated in Fig. 6. The

Table II. Hyperfine field $B_{\rm hf}^{\rm Ru}$ values and the quadrupole splittings at the ^{101}Ru sites.

	$B_{\rm hf}^{\rm Ru}$ (T)	$\lvert(\nu_q/2)(3\cos^2\phi-1)\rvert$ (MHz)
Ru_1	29.8	≤ 0.5
Ru_2	30.7	1
Ru_3	33.3	5
Ru_4	34.9	2

small values of the quadrupole splitting for these sites are consistent with the small line widths of the $^{99}Ru_1$ and $^{99}Ru_2$ sites. Finally, a large quadrupole splitting is expected for the $^{101}Ru_3$ sites because the $^{99}Ru_3$ sites show the largest width. There is indeed a yet unidentified broad peak at 84 MHz, which must be assigned to the highest frequency quadrupole satellite ($M = 5/2$) for the $^{101}Ru_3$ sites. The quadrupole splitting for $^{101}Ru_3$ is then determined to be 5 MHz, generating other satellite lines. The values of the quadrupole splitting for all ^{101}Ru sites are listed in Table II.

The above analysis of the zero-field NMR spectra indicates that all four Ru sites have similar magnitudes of the hyperfine field in the range of 30 - 35 T. Since the hyperfine field at the Ru nuclei $\mathbf{B}_{\rm hf}^{\rm Ru}$ mainly comes from the spin density of the 4*d* states on the same sites, the magnitude of the ordered moments, $\mathbf{m}$, can be determined from the relation

$$\mathbf{B}_{\rm hf}^{\rm Ru} = \mathbf{A}^{\rm Ru} \cdot \mathbf{m} \tag{9}$$

once the hyperfine coupling tensor $\mathbf{A}^{\rm Ru}$ is known. Unfortunately, we were unable to determine $\mathbf{A}^{\rm Ru}$ in $Hg_2Ru_2O_7$, because the Ru NMR signal could not be observed in the paramagnetic phase probably owing to too short a spin-echo decay time. However, the hyperfine field from the 4*d* spin is mostly due to the core-polarization effect, which yields an isotropic coupling constant of -30 ± 6 T/μ_B. This value is basically a single-ion property common to all compounds.[32,33] Using this value, the ordered moments in the antiferromagnetic phase are estimated to be in the range $1.1 \pm 0.3\mu_B$.

Very recently, a magnetic order below $T_{\rm MI}$ has also been detected by muon spin rotation (μSR) experiments.[34] The muon spectrum shows multi-components whose frequencies differ by a factor of three. Since the Ru-NMR results show a largely uniform magnitude of ordered moments, the μSR results indicate either multiple muon sites or multiple internal fields at one crystallographic site due to different degrees of cancellation from neighboring antiferromagnetic moments. The latter is the case for Hg nuclei, as we discussed in §3.1.

If we assume a Mott insulating phase below $T_{\rm MI}$ and take the localized ionic picture with strong correlation, three 4*d* electrons of Ru^{5+} occupying half of the t_{2g} states should form a spin 3/2 with no orbital degree of freedom by the Hund's coupling. We then expect an ordered moment of 3 μ_B per Ru, which is three times larger than the observed value. Neither the deviation of the crystal field from a cubic symmetry in the pyrochlore oxides nor the spin-orbit coupling in 4*d*-transition-metal elements is believed to be strong enough to break the Hund's coupling. Therefore, it appears difficult to explain the small ordered moments by localized spins in the Mott's picture in the strong correlation limit. Localized spin models also seem incompatible with the high transition temperature. An antiferromagnetic order of localized moments on a highly frustrated pyrochlore lattice has to be driven by weak secondary interactions or by partial removal of frustration due to structural distortion. However, neither of these is likely to be sufficient to stabilize the antiferromagnetic order in $Hg_2Ru_2O_7$ up to such a high temperature as $T_{\rm MI} = 107$ K. It thus appears more appropriate to understand the AF insulating state using itinerant electron models. One may argue that a spin-density-wave transition in a three-dimensional pyrochlore lattice is not likely to open a full gap across the entire Fermi surfrace. This is true in the limit of weak correlation. We speculate, however, that moderate correlation effects may open a full gap in the AF state.

The stability of the insulating state in $Hg_2Ru_2O_7$ has been examined theoretically by combining the local-density approximation and the dynamical mean-field theory by Craco *et al.*[27] They found that a significant reduction in the 4*d* electron number as a result of the charge transfer between Ru-O(1) and Hg-O(2) sublattices is necessary to stabilize a paramagnetic insulating state. It should be interesting to examine if the insulating state is stabilized without such a charge transfer in the presence of an antiferromagnetic order. Another point reported by Craco *et al.* is the nearly localized character of the a_{1g} state in contrast to the more itinerant e'_g carrier split by the trigonal crystal field.[27] We note that the antiferromagnetic order of the a_{1g} electrons alone should result in an ordered moment of 1 μ_B.

3.3 Possible magnetic structure

Let us now discuss the magnetic structure below $T_{\rm MI}$. Since spin systems on the pyrochlore lattice with the nearest-neighbor Heisenberg interaction alone remain disordered, magnetic orders induced by various secondary interactions have been studied extensively. Several types of magnetic structures associated with the wave vector $\mathbf{q} = 0$ were found theoretically in the presence of XY-anisotropy,[8] dipolar interaction,[9] and DM interaction.[10] $\mathbf{q} = 0$ magnetic structures were actually observed by neutron scattering experiments, for example, in $Gd_2Sn_2O_7$[35] and $Er_2Ti_2O_7$.[36] The structure in $Gd_2Sn_2O_7$ agrees with the theoretical prediction for a nearest-neighbor Heisenberg antiferromagnet with dipolar interaction.[9] On the other hand, magnetic Bragg peaks with $\mathbf{q} = (1/2, 1/2, 1/2)$ were observed in $Gd_2Ti_2O_7$.[37,38]

The notion of magnetic order stabilized by a weak secondary interaction is probably not relevant to $Hg_2Ru_2O_7$, since the ordered state is stable up to such a high temperature above 100 K. However, knowledge of magnetic structures should still be crucial to understand the mechanism of the MI transition and magnetic order. In the following, we discuss possible spin structures compatible with the NMR data. There are two major observations that put strong constraints on the spin structure: (1) the hyperfine field at one-quarter of the Hg sites is cancelled out, (2) there are four inequivalent Ru

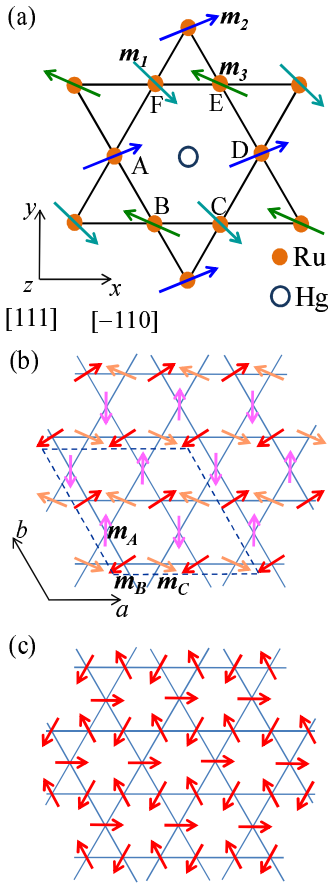


Fig. 7. (Color online) (a) The kagome layer of the Ru pyrochlore lattice with the central Hg site viewed down the [111] direction. An example of the $\mathbf{q} = 0$ spin structure is shown. (b) The antiferromagnetic spin structure within a kagome layer compatible with the NMR results. The dashed line indicates a 2×2 magnetic unit cell. (c) The $\mathbf{q} = 0$ spin structure within a kagome layer that satisfy the cancellation of the hyperfine field at the central Hg nuclei.

sites with different values of $B_{\rm hf}^{\rm Ru}$ and quadrupole splitting. The following discussion is based on the ideal cubic pyrochlore structure and we ignore the small structural distortion in the insulating phase unless explicitly noted otherwise.

We first consider condition (2). The hyperfine field at Ru sites is expressed as $B_{\rm hf}^{\rm Ru} = |\mathbf{A}^{\rm Ru} \cdot \mathbf{m}|$ (eq. 9). If we take only the dominant isotropic part of $\mathbf{A}^{\rm Ru}$ due to the cope polarization effects, $\mathbf{B}_{\rm hf}^{\rm Ru}$ is parallel to $\mathbf{m}$ and $B_{\rm hf}^{\rm Ru}$ depends only on the magnitude of $\mathbf{m}$. Here we consider more general case, where the anisotropic dipolar contribution is included in $\mathbf{A}^{\rm Ru}$. Because of the trigonal symmetry at the Ru sites, $\mathbf{A}^{\rm Ru}$ should be axially symmetric along the ⟨111⟩ direction. Then

$$B_{\rm hf}^{\rm Ru} = m\sqrt{(A_{\parallel}^{\rm Ru})^2 \cos^2\psi + (A_{\perp}^{\rm Ru})^2 \sin^2\psi}, \qquad (10)$$

where ψ is the angle between the trigonal axis and $\mathbf{m}$, and $A_{\parallel}^{\rm Ru}$ ($A_{\perp}^{\rm Ru}$) is the principal values of $\mathbf{A}^{\rm Ru}$ parallel (perpendicular) to the trigonal axis. Thus, $B_{\rm hf}^{\rm Ru}$ depends on both m and ψ. The different values of $B_{\rm hf}^{\rm Ru}$ for the four Ru sites can be due to difference in m or ψ or both.

On the other hand, the relative ratios of the quadrupole splitting $|\nu_q(3\cos^2\phi - 1)|$ among different sites depend only on ϕ since ν_q is common to all Ru sites, though it is unknown. The very small quadrupole splitting at the Ru_1 sites (Table II) suggests that ϕ for Ru_1 is in the neighborhood of the *magic angle*, $\phi = 54.7°$, where $3\cos^2\phi - 1 = 0$. On the other hand, ϕ for the Ru_3 sites with the large splitting should be far from 54.7°. Note that ϕ, which is the angle between the trigonal axis and $\mathbf{B}_{\rm hf}^{\rm Ru}$, is nearly equal to ψ since $\mathbf{A}^{\rm Ru}$ is approximately isotropic.

Next we consider constraints from condition (1). In $Hg_2Ru_2O_7$, both Ru and Hg atoms form distinct pyrochlore lattices. Each pyrochlore lattice consists of two-dimensional kagome and triangular layers alternately stacked along the ⟨111⟩ direction. The kagome layers of the Ru sublattice are coplanar with the triangular layers of the Hg sublattice, which contains one-quarter of the Hg sites. Therefore, it is natural to look for a spin structure in which the hyperfine field at these Hg sites vanishes. Each of these Hg sites has six nearest-neighbor Ru sites on a kagome layer, as shown in Fig. 7(a). These Ru sites are labeled A to F in Fig. 7(a). Since the hyperfine interaction in insulators are short-ranged, we can assume that the hyperfine field at the Hg sites is the sum of the contributions of the six nearest-neighbor Ru sites,

$$\mathbf{B}_{\rm hf}^{\rm Hg} = \sum_{i=A}^{F} \mathbf{A}_i^{\rm Hg} \cdot \mathbf{m}_i, \qquad (11)$$

where $\mathbf{A}_i^{\rm Hg}$ is the hyperfine coupling tensor between the Hg nucleus at the center of the hexagon and the magnetic moment $\mathbf{m}_i$ of the i-th Ru site ($i = A, \ldots, F$). Since the x-axis connecting the A site and the central Hg nucleus has a C_2 symmetry, it is one of the principal axes of $\mathbf{A}_A^{\rm Hg}$, which can be expressed as

$$\mathbf{A}_A^{\rm Hg} = \begin{pmatrix} A_{xx} & 0 & 0 \\ 0 & A_{yy} & A_{yz} \\ 0 & A_{yz} & A_{zz} \end{pmatrix}, \qquad (12)$$

using the xyz-coordinate shown in Fig. 7(a). The hyperfine coupling tensors for the C and E sites are obtained using successive 120 degree rotations,

$$\mathbf{A}_C^{\rm Hg} = \begin{pmatrix} \frac{1}{4}A_{xx} + \frac{3}{4}A_{yy} & -\frac{\sqrt{3}}{4}(A_{xx} - A_{yy}) & -\frac{\sqrt{3}}{2}A_{yz} \\ -\frac{\sqrt{3}}{4}(A_{xx} - A_{yy}) & \frac{3}{4}A_{xx} + \frac{1}{4}A_{yy} & -\frac{1}{2}A_{yz} \\ -\frac{\sqrt{3}}{2}A_{yz} & -\frac{1}{2}A_{yz} & A_{zz} \end{pmatrix},$$

$$\mathbf{A}_E^{\rm Hg} = \begin{pmatrix} \frac{1}{4}A_{xx} + \frac{3}{4}A_{yy} & \frac{\sqrt{3}}{4}(A_{xx} - A_{yy}) & \frac{\sqrt{3}}{2}A_{yz} \\ \frac{\sqrt{3}}{4}(A_{xx} - A_{yy}) & \frac{3}{4}A_{xx} + \frac{1}{4}A_{yy} & -\frac{1}{2}A_{yz} \\ \frac{\sqrt{3}}{2}A_{yz} & -\frac{1}{2}A_{yz} & A_{zz} \end{pmatrix}. \qquad (13)$$

Since pairs of sites B and E, D and A, and F and C are related each other by inversion with respect to the central Hg sites, their coupling tensors are identical; $\mathbf{A}_B^{\rm Hg} = \mathbf{A}_E^{\rm Hg}$, $\mathbf{A}_D^{\rm Hg} = \mathbf{A}_A^{\rm Hg}$, and $\mathbf{A}_F^{\rm Hg} = \mathbf{A}_C^{\rm Hg}$.

One simple way to cancel out the hyperfine field at the central Hg site is to place antiparallel moments with equal magnitudes on every pair of sites related by inversion:

$$\mathbf{m}_A = -\mathbf{m}_D, \ \mathbf{m}_B = -\mathbf{m}_E, \ \mathbf{m}_C = -\mathbf{m}_F. \qquad (14)$$

Since the hyperfine coupling tensors are the same within each pair, the total hyperfine field is zero. An example of such a spin structure is shown in Fig. 7(b). Here, the magnitude and directions of the three moments, $\mathbf{m}_A$, $\mathbf{m}_B$, and $\mathbf{m}_C$, in a kagome layer can be chosen in an arbitrary manner. In addition, the moments on the triangular layers of the Ru pyrochlore sublattice can still be freely choosen. It is obvious that this model provides sufficient freedom to reproduce the zero-field Ru-NMR spectrum (condition 1). Furthermore, if the moments on the triangular layer are aligned uniformly within one layer and oppositely directed on the neighboring triangular layers, the cancellation of the hyperfine field is valid even if the transferred hyperfine interactions up to the third neighbors are considered.

The spin structure of a single kagome layer considered here is described by multiple q-vectors consisting of $\mathbf{q}_1 = (1/2, 0)$, $\mathbf{q}_2 = (0, 1/2)$, and $\mathbf{q}_3 = (1/2, 1/2)$, where the lattice unit vector $\mathbf{a} = [1, 0]$ and $\mathbf{b} = [0, 1]$ of the kagome lattice are defined as shown in Fig. 7(b). For example, the structure shown in Fig. 7(b) is expressed as

$$\begin{aligned}\mathbf{m}(\mathbf{r}) = {} & \mathbf{m}_A \left[\sin\left(2\pi\mathbf{Q}_{3a}\cdot\mathbf{r}\right) + \sin\left(2\pi\mathbf{Q}_{3b}\cdot\mathbf{r}\right)\right]/2 \\ & + \mathbf{m}_B \left[\cos\left(2\pi\mathbf{Q}_{1a}\cdot\mathbf{r}\right) + \cos\left(2\pi\mathbf{Q}_{1b}\cdot\mathbf{r}\right)\right]/2 \\ & + \mathbf{m}_C \left[\cos\left(2\pi\mathbf{Q}_{2a}\cdot\mathbf{r}\right) - \cos\left(2\pi\mathbf{Q}_{2b}\cdot\mathbf{r}\right)\right]/2, \quad (15)\end{aligned}$$

where $\mathbf{Q}_{1a} = (1/2, 0)$, $\mathbf{Q}_{1b} = (1/2, 1)$, $\mathbf{Q}_{2a} = (0, 1/2)$, $\mathbf{Q}_{2b} = (1, 1/2)$, $\mathbf{Q}_{3a} = (1/2, 1/2)$, $\mathbf{Q}_{3b} = (-1/2, 1/2)$. Of course, other structures are also possible. The condition eq. (14) requires that the ordering wave vector of the A-sublattice is either $\mathbf{q}_1$ or $\mathbf{q}_2$. Likewise, the ordering of the B (C)-sublattice must have the wave vector $\mathbf{q}_1$ or $\mathbf{q}_3$ ($\mathbf{q}_2$ or $\mathbf{q}_3$). In all the cases, the magnetic unit cell is 2×2 times larger than the crystaline unit cell, as shown by the dashed line in Fig. 7(b). However, to our knowledge, such magnetic structures have not been observed in materials containing kagome or pyrochlore lattices.

We also examined simpler structures in a single kagome layer with $\mathbf{q} = 0$, which conserve the translational symmetry of the kagome lattice, as shown in Fig. 7(a). In this case, the requirement that the hyperfine field at the central Hg site should vanish under general conditions (not by coincidence) completely determines the spin structure, as shown in Fig. 7(c). Here, the moments on a kagome layer are directed perpendicular to the mirror plane, forming a 120 degree structure. Details of this analysis are presented in the appendix. This is the structure proposed for the kagome layers of $Gd_2Ti_2O_7$ in ref. 37, where the spins on the triangular layers are reported to remain disordered. We should note that this structure for a single kagome layer is compatible with the Bragg peak at $\mathbf{q} = (1/2, 1/2, 1/2)$ of the cubic pyrochlore structure observed in $Gd_2Ti_2O_7$.[37] It should also be mentioned that subsequent experiments[38]revealed that the antiferromagnetic order in the ground state of $Gd_2Ti_2O_7$ has a 4-k structure, not the single k structure considered here.

The structure shown in Fig. 7(c), however, is not compatible with the NMR observation of four inequivalent Ru sites, unless the lowering of the crystal symmetry due to structural transition is explicitly considered. Since all the moments on the kagome layers, $\mathbf{m}_1$, $\mathbf{m}_2$, and $\mathbf{m}_3$, are perpendicular to the trigonal axes of their respective sites, $\phi = \psi = 90°$, three Ru sites must have the same quadrupole splitting equal to $|\nu_q/2|$. Even the fourth Ru sites on the triangular layers have different quadrupole splitting, only two sites are allowed in this structure. More quantitatively, the results in Table II impose $|\nu_q|$, which is the possible maximum quadrupole splitting, to be equal or larger than 5 MHz, which is the largest quadrupole splitting observed at the Ru_3 sites. Therefore, $|\nu_q/2| \geq 2.5$ MHz. However, this value is considerably larger than the quadrupole splitting at any other site (see Table II). In principle, the structural distortion observed below $T_{\rm MI}$ may change the EFG and break the symmetry of the hyperfine coupling tensors shown in eqs. (12) and (13), allowing four distinct sites. However, the small lattice distortion observed in $Hg_2Ru_2O_7$ appears to be insufficient to resolve the large quantitative discrepancy.

In the above discussion, we have not considered explicitly the presence of two inequivalent sites within one-quarter of the Hg sites with cancelled hyperfine fields, as shown in Fig. 4. Such a subtle distinction could be due to the structural distortion in the insulating phase. Detailed structural analysis would be necessary to understand the origin of the two inequivalent Hg sites.

4. Summary

We have presented the ^{199}Hg- and ^{99,101}Ru-NMR results of the pyrochlore oxide $Hg_2Ru_2O_7$. In the metallic phase above $T_{\rm MI}$, the nuclear spin-lattice relaxation rate $1/T_1$ and the magnetic shift at the ^{199}Hg sites follow the Korringa relation, which indicates the absence of spatial magnetic correlations. Below $T_{\rm MI}$, ^{99,101}Ru-NMR lines are observed at zero field, providing evidence for a commensurate antiferromagnetic order. This is in contrast to the singlet ground state of another pyrochlore oxide showing a MI transition $Tl_2Ru_2O_7$. The ordered moments are estimated to be about $1\mu_B$. The reduced moment compared with the ionic value implies that localized spin models with strong Hund's coupling are inadequate. An itinerant electron model may be more appropriate to understand the magneic properties of $Hg_2Ru_2O_7$ even below $T_{\rm MI}$. Possible magnetic structures compatible with the NMR results were proposed. It would be a future theoretical challenge to examine the stability of specific antiferromagnetic structures in the insulating state.

Acknowledgment

We thank Hisatomo Harima for informing us of the results of his LDA calculation. This work was supported by MEXT KAKENHI on Priority Areas "Novel State of Matter Induced by Frustration" (Nos. 22014004 and 19052008) and JSPS KAKENHI (B) (No. 21340093) and (C) (No. 50398898).

Appendix: $q = 0$ antiferromagnetic structure in a kagome layer

We consider possible spin structures with $\mathbf{q} = 0$ under the condition that a hyperfine field at Hg nuclei on the kagome layer of the Ru pyrochlore sublattice cancels out.

A $\mathbf{q} = 0$ structure on a kagome layer is illustrated in Fig. 7(a). We define the components of the sublattice moments as

$$\begin{aligned}\mathbf{m}_C &= \mathbf{m}_F = \mathbf{m}_1 = (m_x^1, m_y^1, m_z^1)\\ \mathbf{m}_A &= \mathbf{m}_D = \mathbf{m}_2 = (m_x^2, m_y^2, m_z^2)\\ \mathbf{m}_B &= \mathbf{m}_E = \mathbf{m}_3 = (m_x^3, m_y^3, m_z^3).\end{aligned} \tag{A·1}$$

The hyperfine field at the central Hg site is given by

$$\begin{aligned}\mathbf{B}_{\rm hf}^{\rm Hg} =&(\mathbf{A}_C^{\rm Hg} + \mathbf{A}_F^{\rm Hg})\cdot\mathbf{m}_1\\ &+\ (\mathbf{A}_A^{\rm Hg} + \mathbf{A}_D^{\rm Hg})\cdot\mathbf{m}_2\\ &+\ (\mathbf{A}_B^{\rm Hg} + \mathbf{A}_E^{\rm Hg})\cdot\mathbf{m}_3.\end{aligned} \tag{A·2}$$

Each component of $\mathbf{B}_{\rm hf}^{\rm Hg} = (B_x, B_y, B_z)$ can be written as

$$\begin{aligned}B_x =& \left(\frac{1}{2}m_x^1 - \frac{\sqrt{3}}{2}m_y^1 + 2m_x^2 + \frac{1}{2}m_x^3 + \frac{\sqrt{3}}{2}m_y^3\right)A_{xx}\\ &+\left(\frac{3}{2}m_x^1 + \frac{\sqrt{3}}{2}m_y^1 + \frac{3}{2}m_x^3 - \frac{\sqrt{3}}{2}m_y^3\right)A_{yy}\\ &+\left(-\sqrt{3}m_z^1 + \sqrt{3}m_z^3\right)A_{yz},\\ B_y =& \left(-\frac{\sqrt{3}}{2}m_x^1 + \frac{3}{2}m_y^1 + \frac{\sqrt{3}}{2}m_x^3 + \frac{3}{2}m_y^3\right)A_{xx}\\ &+\left(\frac{\sqrt{3}}{2}m_x^1 + \frac{1}{2}m_y^1 + 2m_y^2 - \frac{\sqrt{3}}{2}m_x^3 + \frac{1}{2}m_y^3\right)A_{yy}\\ &+\left(-m_z^1 + 2m_z^2 - m_z^3\right)A_{yz},\\ B_z =& \left(-\sqrt{3}m_x^1 - m_y^1 + 2m_y^2 + \sqrt{3}m_x^3 - m_y^3\right)A_{yz}\\ &+\left(2m_z^1 + 2m_z^2 + 2m_z^3\right)A_{zz}.\end{aligned} \tag{A·3}$$

The condition $\mathbf{B}_{\rm hf}^{\rm Hg} = 0$ for general values of A_{xx}, A_{yy}, A_{zz}, and A_{yz} requires the following:

$$\frac{1}{2}m_x^1 - \frac{\sqrt{3}}{2}m_y^1 + 2m_x^2 + \frac{1}{2}m_x^3 + \frac{\sqrt{3}}{2}m_y^3 = 0 \tag{A·4}$$

$$\frac{3}{2}m_x^1 + \frac{\sqrt{3}}{2}m_y^1 + \frac{3}{2}m_x^3 - \frac{\sqrt{3}}{2}m_y^3 = 0 \tag{A·5}$$

$$-\sqrt{3}m_z^1 + \sqrt{3}m_z^3 = 0 \tag{A·6}$$

$$-\frac{\sqrt{3}}{2}m_x^1 + \frac{3}{2}m_y^1 + \frac{\sqrt{3}}{2}m_x^3 + \frac{3}{2}m_y^3 = 0 \tag{A·7}$$

$$\frac{\sqrt{3}}{2}m_x^1 + \frac{1}{2}m_y^1 + 2m_y^2 - \frac{\sqrt{3}}{2}m_x^3 + \frac{1}{2}m_y^3 = 0, \tag{A·8}$$

$$-m_z^1 + 2m_z^2 - m_z^3 = 0 \tag{A·9}$$

$$-\sqrt{3}m_x^1 - m_y^1 + 2m_y^2 + \sqrt{3}m_x^3 - m_y^3 = 0 \tag{A·10}$$

$$2m_z^1 + 2m_z^2 + 2m_z^3 = 0. \tag{A·11}$$

From eqs. (A· 6), (A· 9), and (A· 11), we obtain

$$m_z^1 = m_z^2 = m_z^3 = 0, \tag{A·12}$$

which means that the moments should lie within the kagome layer.

Equations. (A· 7) and (A· 4) can be rewitten as

$$-\frac{1}{2}m_x^1 + \frac{\sqrt{3}}{2}m_y^1 = -\frac{1}{2}m_x^3 - \frac{\sqrt{3}}{2}m_y^3 = m_x^2. \tag{A·13}$$

Likewise, from eqs. (A· 5) and (A· 8) we obtain

$$-\frac{\sqrt{3}}{2}m_x^1 - \frac{1}{2}m_y^1 = \frac{\sqrt{3}}{2}m_x^3 - \frac{1}{2}m_y^3 = m_y^2. \tag{A·14}$$

These equations can be combined in a matrix form as

$$\begin{aligned}\begin{pmatrix} m_x^2 \\ m_y^2 \end{pmatrix} &= \begin{pmatrix} -1/2 & \sqrt{3}/2 \\ -\sqrt{3}/2 & -1/2 \end{pmatrix}\begin{pmatrix} m_x^1 \\ m_y^1 \end{pmatrix}\\ \begin{pmatrix} m_x^2 \\ m_y^2 \end{pmatrix} &= \begin{pmatrix} -1/2 & -\sqrt{3}/2 \\ \sqrt{3}/2 & -1/2 \end{pmatrix}\begin{pmatrix} m_x^3 \\ m_y^3 \end{pmatrix}.\end{aligned} \tag{A·15}$$

Thus, $\mathbf{m}_1$, $\mathbf{m}_2$, and $\mathbf{m}_3$ are related by successive 120 degree rotations within the kagome layer. Finally, by combining eqs. (A· 10) and (A· 14), we obtain

$$m_y^2 = 0. \tag{A·16}$$

Therefore, the spin structure is uniquely determined as illustrated in Fig. 7(c).

1) For a review, see J. S. Gardner, K. J. P. Gingras, and J. E. Greedan: Rev. Mod. Phys. **82** (2010) 53.
2) J. N. Reimers: Phys. Rev. B **45** (1992) 7287.
3) R. Moessner and J. T. Chalker: Phys. Rev. B **58** (1998) 12049.
4) R. Moessner and J. T. Chalker: Phys. Rev. Lett. **80** (1998) 2929.
5) B. Canals and C. Lacroix: Phys. Rev. Lett. **80** (1998) 2933.
6) B. Canals and C. Lacroix: Phys. Rev. B **61** (2000) 1149.
7) H. Tsunetsugu: Phys. Rev. B **65** (2001) 024415.
8) S. T. Bramwell and M. J. P. Gingras: J. Appl. Phys. **75** (1994) 5523.
9) S. E. Palmer and J. T. Chalker: Phys. Rev. B **62** (2000) 488.
10) M. Elhajal, B. Canals, R. Sunyer, and C. Lacroix: Phys. Rev. B **71** (2005) 094420.
11) Y. Yamashita and K. Ueda: Phys. Rev. Lett. **85** (2000) 4960.
12) O. Tchernyshyov, R. Moessner, and S. L. Sondhi: Phys. Rev. B **66** (2002) 064403.
13) S. Kondo, D. C. Johnston, C. A. Swenson, F. Borsa, A. V. Mahajan, L. L. Miller, T. Gu, A. I. Goldman, M. B. Maple, D. A. Gajewski, E. J. Freeman, N. R. Dilley, R. P. Dickey, J. Merrin, K. Kojima, G. M. Luke, Y. J. Uemura, O. Chmaissem, and J. D. Jorgensen: Phys. Rev. Lett. **78** (1997) 3729.
14) C. Urano, M. Nohara, S. Kondo, F. Sakai, H. Takagi, T. Shiraki, and T. Okubo: Phys. Rev. Lett. **85** (2000) 1052.
15) A. W. Sleight, J. L. Gillson, j. F. Weiher, and W. Bindloss: Solid State Commun. **14** (1974) 357.
16) D. Mandrus, J. R. Thompson, R. Gaal, L. Forro, J. C. Bryan, B. C. Chakoumakos, L. M. Woods, B. C. Sales, R. S. Fishman, and V. Keppens: Phys. Rev. B **63** (2001) 195104.
17) T. Takeda, R. Kanno, Y. Kawamoto, M. Takano, F. Izumi, A. W. Sleight, and A. W. Hewat: J. Mater. Chem. **9** (1999) 215.
18) H. Sakai, M. Kato, K. Yoshimura, and K. Kosuge: J. Phys. Soc. Jpn. **71** (2002) 422.
19) S. Lee, J.-G. Park, D. T. Adroja, D. Khomski, S. Streltsov, K. A. McEwen, H. Sakai, K. Yoshimura, V. I. Anisimov, D. Mori, R. Kanno, and R. Ibberson: Nat. Mater. **5** (2006) 471.
20) A. Yamamoto, P. A. Sharma, Y. Okamoto, A. Nakao, H. A. Katori, S. Niitaka, D. Hashizume, and H. Takagi: J. Phys. Soc. Jpn. **76** (2007) 043703.
21) W. Klein, R. K. Kremer, and M. Jansen: J. Mater. Chem. **17** (2007) 1356.
22) N. Takeshita, C. Terakura, Y. Tokura, A. Yamamoto, and H. Takagi: J. Phys. Soc. Jpn. **76** (2007) 063707.

23) W. G. Clark, M. E. Hanson, F. Lefloch, and P. Shgransan: Rev. Sci. Instrum. **66** (1995) 2453.
24) R. G. Kidd and R. J. Goodfellow: in *NMR and the Periodic Table,* ed. R. K. Harris and B. E. Mann (Academic Press, London 1978).
25) T. Moriya: *Spin Fluctuations in Itinerant Electron Magnetism*; Springer Series in Solid State Science **56** (Springer, 1985).
26) A. J. Millis, H. Monien, and D. Pines: Phys. Rev. B **42** (1990) 167.
27) L. Craco, M. S. Laad, S. Leoni, and H. Rosner: Phys. Rev. B **79** (2009) 075125.
28) H. Harima: private communications.
29) H. Shiba: Prog. Theor. Phys. **54** (1975) 967.
30) In evaluating the integrated intensity of the spectra in Fig. 3, the effect of spin-echo decay is corrected by extrapolating the integrated intensity to $\tau = 0$, where τ is the separation between the $\pi/2$ and π pulses in the spin-echo pulse sequence.
31) Although the cubic symmetry of the pyrochlore structure is actually broken in the insulating phase of $Hg_2Ru_2O_7$, the EFG at the Ru sites should still be approximately axially symmetric since the structural distortion is quite small.[20]
32) R. E. Watson and A. J. Freeman: in *Hyperfine Interaction,* ed. A. J. Freeman and R. B. Frankel (Academic Press, New York, 1967) Chap. 2, p. 53.
33) H. Mukuda, K. Ishida, Y. Kitaoka, K. Asayama, R. Kanno, and M. Takano: Phys. Rev. B **60** (1999) 12279.
34) M. Miyazaki, R. Kadono, K. H. Satoh, M. Hiraishi, S. Takeshita, A. Koda, A. Yamamoto, and H. Takagi: Phys. Rev. B **82** (2010) 094413.
35) A. S. Wills, M. E. Zhitomirsky, B. Canals, J. P. Sanchez, P. Bonville, P. Dalmas de Réotier, and A. Yaouanc: J. Phys.: Condens Matter **18** (2006) L37.
36) A. Poole, A. S. Wills, and E. Leliévre-Berna: J. Phys.: Condens Matter **19** (2007) 452201.
37) J. D. M. Champion, A. S. Wills, T. Fennell, S. T. Bramwell, J. S. Gardner, and M. A. Green: Phys. Rev. B **64** (2001) 140407(R).
38) J. R. Stewart, G. Ehlers, A. S. Wills, S. T. Bramwell, and J. S. Gardner: J. Phys.: Condens Matter **16** (2004) L321.